Velocity space evolution of a minority energetic electron population undergoing the anomalous Doppler instability

W. N. Lai, S. C. Chapman, and R. O. Dendy

Citation: Physics of Plasmas **22**, 112119 (2015); doi: 10.1063/1.4936101
View online: http://dx.doi.org/10.1063/1.4936101
View Table of Contents: http://scitation.aip.org/content/aip/journal/pop/22/11?ver=pdfcov
Published by the AIP Publishing

Velocity space evolution of a minority energetic electron population undergoing the anomalous Doppler instability

W. N. Lai,[1] S. C. Chapman,[1,a)] and R. O. Dendy[1,2]
[1]Centre for Fusion, Space and Astrophysics, Department of Physics, University of Warwick, Coventry, United Kingdom
[2]CCFE, Culham Science Centre, Abingdon, Oxfordshire OX14 3DB, United Kingdom

(Received 6 July 2015; accepted 3 November 2015; published online 30 November 2015)

The kinetic evolution in velocity space of a minority suprathermal electron population that is undergoing the anomalous Doppler instability (ADI) is investigated using the results from fully nonlinear numerical simulations that self-consistently evolve particles and fields in a plasma. Electron trajectories in phase space during different stages of the ADI are captured, and are analysed in relation to the characteristics of the excited electric fields and of the overall distribution of particles. For some electrons, trapping and mirroring effects are observed during the saturation phase. A relationship between the second order moments of the perpendicular electron distribution function and time is established, and is used to investigate the range of applicability of analytical approximations drawn from classical theory, that involve a quasilinear wave-driven diffusion operator. [http://dx.doi.org/10.1063/1.4936101]

I. INTRODUCTION

The anomalous Doppler instability (ADI)[1–16] is a key collective relaxation mechanism for minority suprathermal electron populations in magnetically confined fusion plasmas. Through the ADI, excess parallel kinetic energy is converted into perpendicular kinetic energy together with the field energy of excited waves. This rests on wave-particle resonance between electrons and waves that satisfy the anomalous Doppler resonance criterion

$$\omega_k + \Omega_{ce} = k_{\|} v_{\|}, \tag{1}$$

where ω_k is the frequency if the excited waves, Ω_{ce} is the electron cyclotron frequency, $k_{||}$ is the wavenumber parallel to the external magnetic field and $v_{||}$ is the parallel component of the velocity of the resonant electrons. Relaxation of energetic electron populations through the ADI is of substantial practical interest for contemporary tokamak plasmas.[10–12,17,18] Most recently, it appears that the ADI is playing a key role in the fast evolution of the electron population during the early stages of edge localised modes (ELMs) in MAST.[19] The ADI is also believed to operate in space plasmas,[15,20] and the ADI is a close relative of the instability at the inner Lindblad resonance in galactic dynamics.[21]

Early analytical studies of the ADI rested on the properties of the linear growth rate.[8] These were sometimes combined[22] with model quasilinear wave-driven diffusion operators, to provide an indicative guide to the evolution in velocity space of the energetic electron population. It has only recently become possible to transcend the limitations of this approach. A particle-in-cell (PIC) code[23] was used[9] to calculate the fully self-consistent nonlinear evolution of kinetic electron dynamics and electromagnetic fields undergoing the ADI for tokamak-relevant parameter regimes. This study provided a systematic account of the extent to which the linear analytical theory of ADI growth provides a guide to the fully nonlinear ADI, and of the character of the waves that are excited.

In the present paper we therefore turn to the second aspect of ADI physics that is important for experimental interpretation: the evolution in time of the distribution of energetic electrons in velocity space, which takes the form of a fan-like spreading by which a "tail," oriented initially along the magnetic field direction, becomes a "pancake." For experimental applications of ADI theory, it would be helpful to identify how the fully self-consistent relativistic nonlinear PIC simulation of the ADI diverges from a quasilinear approximation.

To investigate these questions we use a fully relativistic PIC code which self-consistently solves the Lorentz-Maxwell system of equations for many millions of kinetic electrons together with the full vector electric and magnetic fields. Our simulations have one spatial dimension x, which can be oriented arbitrarily with respect to the direction of the background magnetic field, and three velocity co-ordinates for the particles. A consequence of the fact that PIC codes operate at the level of description of kinetic particles and fields is that there are no ab initio assumptions about the presence or character of wave modes, if any. Instead the character of any waves is inferred from the simulation results, by means of spatio-temporal Fourier transforms of the electric and magnetic fields that arise. Similarly, no explicit wave-particle interactions are imposed at the PIC level of description of the plasma. Wave-particle interactions are higher order phenomena, which are inferred from the simulation results using ensembles of particle orbits, the particle distribution function, and the spatio-temporal Fourier transforms of the electric and magnetic fields. In our simulations here, as in Ref. 9, we find empirically that Landau damping is the dominant among the damping mechanisms that are possible in principle,[25] as is assumed in most

a)Electronic mail: S.C.Chapman@warwick.ac.uk

analytical treatments. Again empirically, particles at anomalous Doppler wave-particle resonance drive the instability.

As in Ref. 9, we use the EPOCH (Extendable PIC Open Collaboration) PIC code[23,24] which has been extensively benchmarked in nonlinear plasma physics regimes by its large user community. In general PIC code benchmarking in fully nonlinear regimes is achieved by simulating structures such as shocks and solitons for which analytical solutions exist, and by varying cell sizes and particle step lengths, and iterating until convergence is obtained. The self-consistent phase space dynamics of each kinetic particle is evolved in combination with the spatiotemporal evolution of the electric and magnetic fields, with periodic boundary conditions. Grid cell sizes are such that the simulations fully resolve the lengthscales that characterise electron dynamics, including Debye length and gyro-radius. The details of the simulation and initial setup are given in Ref. 9, and the initial conditions are similar to those in Ref. 9 with a few changes. The simulation results here were obtained using tokamak-relevant parameters that would generically characterise, for example, the outer region of a medium-size tokamak; see, for example, the profiles for Tore Supra shown in Fig. 4 of Ref. 26. The initial bulk electron and ion temperatures are set equal at 1.0 keV, and the value of the bulk electron number density is $1.0\times10^{19}\,\mathrm{m}^{-3}$. The electron tails are mildly relativistic. The parallel velocity of the suprathermal electron tail distribution extends up to $2.5\times10^{8}\,\mathrm{ms}^{-1}$. In this mildly relativistic regime, the flat tail electron distribution in velocity space is monotonically decreasing in momentum space. We recall that, distinctively among collective instabilities, the ADI can occur in the absence of a positive slope of the particle distribution anywhere in velocity space.

II. QUASI-LINEAR ANALYSIS

The quasilinear equation for wave-particle resonant diffusion in velocity space for a uniform magnetised plasma was first derived by Kennel and Engelmann from the Vlasov equation.[27] The relativistic generalisation of the quasilinear model is due to several authors, see for example, the works by Kulsrud and Ferrari[28] and Stix[29] and references therein. In the present paper, we will compare the results of direct numerical PIC simulation of the fully nonlinear ADI with the output from two widely used quasi-linear equations.[30–36] In regimes where the quasilinear approach is found to approximate well to the PIC code, it can reasonably be adopted in models for use in experimental interpretation. The first quasi-linear equation of interest is adopted from Ref. 32

$$\frac{\partial f}{\partial t}=\int d^3k\left[\frac{l\Omega_{ce}}{v_\perp}\frac{\partial}{\partial v_\perp}\left(D\hat{\Pi}f\right)+\frac{\partial}{\partial v_\parallel}\left(k_\parallel D\hat{\Pi}f\right)\right]. \tag{2}$$

Here f is the electron distribution function; Ω_{ce} is the electron cyclotron frequency; l is the dominant cyclotron resonant harmonic ($l=-1$ for the ADI); ($v_{||}$, $v_\perp$) are the parallel and perpendicular velocity with respect to the magnetic field direction; and $k_{||}$ is the wavenumber parallel to the external magnetic field. The operator $\hat{\Pi}$ is the pitch angle gradient operator, and is defined as

$$\hat{\Pi}=\frac{l\Omega_{ce}}{v_\perp}\frac{\partial}{\partial v_\perp}+k_\parallel\frac{\partial}{\partial v_\parallel}. \tag{3}$$

The coefficient D can be expressed as

$$D=\frac{\pi e^2}{m_0^2}\frac{|\mathbf{E}_{k_\parallel}|^2}{\omega_k^2}\sum_{l=-\infty}^{\infty}\delta\left(\omega_k-l\Omega_{ce}-k_\parallel v_\parallel\right)|\hat{\mathbf{e}}_k\cdot\mathbf{V}|^2, \tag{4}$$

where $|\mathbf{E}_{k_\parallel}|$ is the electric field amplitude of the waves along the external magnetic field. In Eq. (4), m_0 and e are the electron rest mass and charge, respectively, ω_k is the angular frequency of the wave, $\hat{\mathbf{e}}_k$ is the unit directional vector along the wave vector $\mathbf{k}$, and the vector $\mathbf{V}$ is defined as

$$\mathbf{V}=\begin{pmatrix}\frac{1}{2}v_\perp\left(e^{i\phi}J_{l-1}(z)+e^{-i\phi}J_{l+1}(z)\right)\\ \frac{1}{2i}v_\perp\left(e^{i\phi}J_{l-1}(z)+e^{-i\phi}J_{l+1}(z)\right)\\ v_\parallel J_l(z)\end{pmatrix}. \tag{5}$$

Here ϕ is the phase of circularly polarised waves, J_l is the Bessel function of order l, and the argument of the Bessel function is $z=k_\perp v_\perp/\Omega_{ce}$. The delta function in the operator D in Eq. (4) represents wave-particle interactions, which pick out the parallel particle velocity $v_{||}$ that resonates with the waves. The second quasilinear equation of interest, Eq. (6),[37,38] is similar to Eq. (2) apart from a few differences.[34,35] First, $k_{||}$ is not subject to the differential operator in the second term of Eq. (2); and second, Eq. (6) considers the relativistic limit. For wave-particle interactions, $k_{||}$ usually has a strong dependence on $v_{||}$, however it will be shown in a later section that for the relativistic case and under certain assumptions, such dependence is unimportant. The second quasilinear formulation is written as

$$\frac{\partial f}{\partial t}=\int d^3k\hat{\Pi}_R D_R\hat{\Pi}_R f, \tag{6}$$

where the operator $\hat{\Pi}_R$ has a slightly different definition from that of $\hat{\Pi}$ given in Eq. (3)

$$\hat{\Pi}_R=\frac{l\Omega_{ce}}{v_\perp}\frac{\partial}{\partial v_\perp}+\frac{k_\parallel}{\gamma}\frac{\partial}{\partial v_\parallel}, \tag{7}$$

where γ is the Lorentz factor. The function D_R is defined below, and differs slightly from D given in Eq. (4)

$$D_R=\pi e^2\sum_{l=-\infty}^{\infty}p_\perp^2\frac{|\Psi_{l,k}|^2}{\omega_k^2}\delta\left(\omega_k-l\Omega_{ce}-k_\parallel v_\parallel\right). \tag{8}$$

Here $|\Psi_{l,k}|^2$ is defined as

$$|\Psi_{l,k}|^2=\left|E_{k_{\perp1}}\frac{l}{z}J_l(z)+iE_{k_{\perp2}}J_l'(z)+\frac{p_\parallel}{p_\perp}E_{k_\parallel}J_l(z)\right|^2, \tag{9}$$

where $(E_{k_{\perp1}},E_{k_{\perp2}},E_{k_\parallel})$ are the electric field components perpendicular and parallel to the magnetic field; ($p_{||}$, $p_\perp$) are the parallel and perpendicular momentum; $J_l'(z)$ denotes the

derivative of the Bessel function; and the argument z has the same definition as before.

Considering electrostatic waves and assuming that $k_{\|}\partial f/\partial v_{\|} \ll (\Omega_{ce}/v_{\perp})\partial f/\partial v_{\perp}$ and $v_{||} \simeq c$, Eq. (6) can be simplified to Eq. (10) below[34]

$$\frac{\partial f}{\partial t} = \frac{1}{p_{\perp}}\frac{\partial}{\partial p_{\perp}}\frac{D_p}{p_{\perp}}\frac{\partial}{\partial p_{\perp}}f. \tag{10}$$

Here the diffusion coefficient D_p is given by

$$D_p = \int d^3k \frac{\pi m_0^2 e^2 \Omega_{ce}^2}{k^2} \sum_{l=-\infty}^{\infty} |E_{k_{\|}} J_l(z)|^2 \delta\left(\omega - k_{\|}v_{\|} - l\Omega_{ce}\right). \tag{11}$$

The assumptions leading to Eqs. (10) and (11) are applicable to our simulations below, since $k_{||}v_{\perp}/\Omega_{ce} \ll 1$ and $\partial f/\partial v_{||} \ll \partial f/\partial v_{\perp}$ for the initial flat tail suprathermal electron distribution. The diffusion coefficient D_p is still function of $v_{\perp}$, therefore we expand the Bessel function up to the first order so that Eq. (10) becomes

$$\frac{\partial f}{\partial \tau} = \frac{1}{p_{\perp}}\frac{\partial}{\partial p_{\perp}}p_{\perp}\frac{\partial}{\partial p_{\perp}}f, \tag{12}$$

and the normalised time τ is defined as

$$\tau = \int_0^t dt' \frac{\pi e^2}{4} \int d^3k \frac{k_{\perp}^2}{k^2} |E_{k_{\|}}|^2 \delta\left(\omega_k + \Omega_{ce} - k_{\|}v_{\|}\right). \tag{13}$$

The structure of this paper is as follows. First, we investigate the applicability of the assumptions of the quasilinear theory from the perspective of single particle dynamics as revealed by the fully nonlinear selfconsistent PIC simulations. We then establish a relation between the second order moments of the perpendicular electron distribution function and time, with diffusion coefficients obtained from analytical quasilinear expressions that use the analytical linear growth rate formulated in Ref. 8.

III. RESULTS

A. Trajectories of electrons undergoing ADI

Figure 1 shows four examples of the trajectories, in ($p_{||}$, $p_{\perp}$) momentum space, of tail electrons undergoing the ADI. Initially the electrons have small pitch angles, and they move to higher $p_{\perp}$ at later times. Particles undergoing the ADI lose energy to the excited wave fields, while simultaneously transforming parallel into perpendicular kinetic energy. This is reflected in the initial trajectories of all four particles in Fig. 1, which follow the solid black curve representing the resonance contour, which is the energy conservation contour of an electron taking into account the energy transferred to the excited wave during the ADI in the rest frame of the bulk electrons. During the linear stage of the ADI, which is relevant to this stage of the phase space evolution of the electrons, it is known[4,8] that the ratio of the loss in parallel kinetic energy of an electron $\Delta E_{||}$ to its gain in perpendicular energy $\Delta E_{\perp}$ is $(\Omega_{ce}+\omega_k)/\Omega_{ce}$ (we note that this ratio is found not to apply in the fully nonlinear regime the ADI, see Fig. 10 of Ref. 9). By taking the ratio of the kinetic energy loss of an electron, $\Delta E = \Delta E_{||} - \Delta E_{\perp}$, to the parallel kinetic energy loss $\Delta E_{||}$, we have

$$\frac{\Delta E}{\Delta E_{\|}} = \frac{m\left(v_{\perp}\delta(\gamma v_{\perp}) + v_{\|}\delta(\gamma v_{\|})\right)}{m v_{\|}\delta(\gamma v_{\|})} = \frac{\omega_k}{\Omega_{ce}+\omega_k}. \tag{14}$$

Rearranging the above expression gives the resonance contour for electrons undergoing the ADI[27]

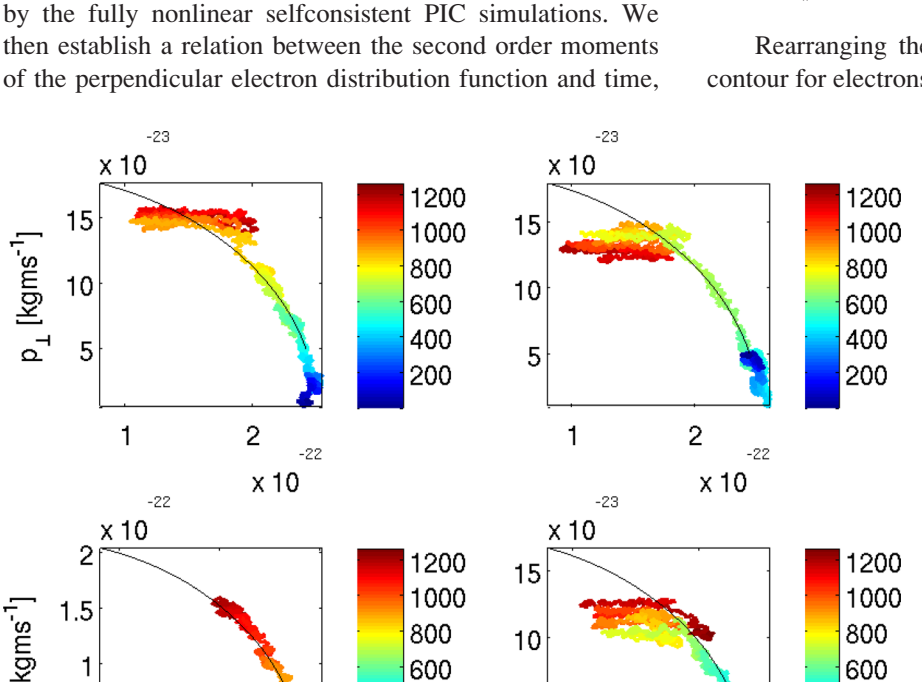

FIG. 1. Panels show trajectories of four different electrons chosen from the suprathermal population, in ($p_{||}$, $p_{\perp}$) momentum space. The colour of dots represents the time in units of cyclotron periods, blue corresponding to earlier times and red to later. The black curves plot the contour of the anomalous Doppler resonance defined by Eq. (15), where the value of C is different in each panel.

$$\left(\frac{\Omega_{ce}}{\Omega_{ce}+\omega_k}\right)p_{\|}^2+p_{\perp}^2=C, \tag{15}$$

where C is a constant. From Fourier analysis of the electric field, it is shown in Fig. 2 that $\omega_k \simeq 0.35\Omega_{ce}$ is the dominant frequency of the excited wave for the parameter values of the simulation. In terms of the linear dispersion relation, this value of ω_k corresponds to the lower electrostatic mode as defined in Ref. 25.

The electron trajectories shown in Fig. 1 can broadly be characterised into three different stages. In the first stage, which lasts for the first hundred cyclotron periods, the electrons have no obvious net displacement in momentum space. This phase corresponds to panels (a)–(c) of Fig. 2 in Ref. 9, during which there is significant excitation of electrostatic waves, see panels (a)–(c) of Fig. 3 of Ref. 9. In the second stage, which lasts several hundred cyclotron periods, the electrons follow the resonance contour defined by Eq. (15) and evolve towards substantially larger $p_\perp$. This phase corresponds to panels (d)–(f) of Fig. 2 in Ref. 9. Finally, in the third stage, the electrons deviate from the resonance contour and, in some cases, mirror back and forth in the $p_{||}$ direction.

In order to quantify the behaviour of the electrons at different stages, we construct the pdf of $\Delta p_\perp$, where $\Delta p_\perp$ is the difference in $p_\perp$ between successive time steps, $\Delta t = 0.17\tau_{ce}$, computed for 20 macroparticles exhibiting similar trajectories to the ones shown in Fig. 1. We label this pdf as $g(\Delta p_\perp)$. The time evolution of the first three moments of $g(\Delta p_\perp)$, namely, its mean, standard deviation and skewness, is shown in Fig. 3. All three moments grow steadily during the early stages of the ADI and peak at approximately $750\tau_{ce}$. This

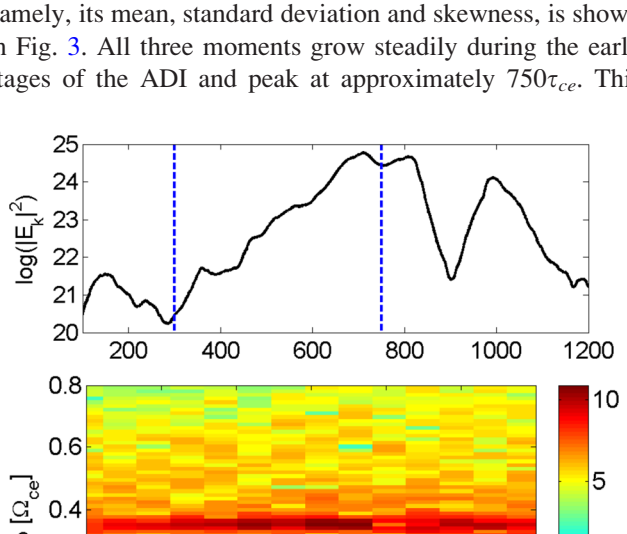

FIG. 2. Time evolution of energy density and frequency structure of the ADI-excited electric fields. Top panel shows the logarithmic electric field amplitude squared for wavenumber, $kv_B/\Omega_{ce} = 0.1245$, plotted against time. Dotted blue lines mark the times, $t = 300\tau_{ce}$ and $t = 750\tau_{ce}$, that separate the three stages of the ADI mentioned in Section III; here τ_{ce} denotes the electron cyclotron period. A. Bottom panel shows the logarithmic density plot of electric field amplitude (red corresponds to higher field amplitude and blue to lower field amplitude) in frequency-time space, $|E_k(\omega,t)|$, for a particular wavenumber $k_\perp v_B/\Omega_{ce} = 0.1225$, where v_B is the thermal velocity of the bulk electrons. The time axes of both panels are in units of the cyclotron period τ_{ce}.

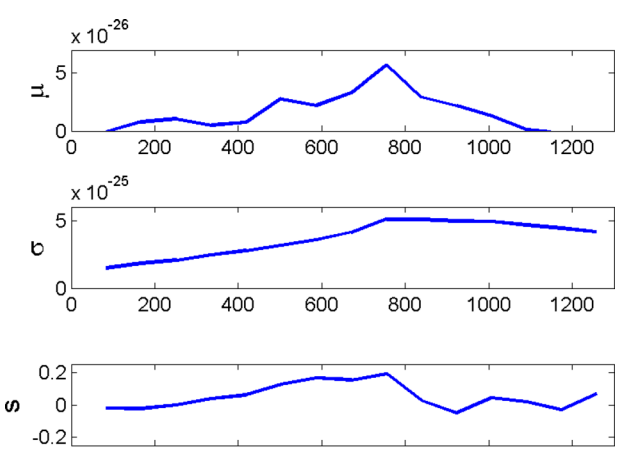

FIG. 3. Time evolution of the moments of the pdf $g(\Delta p_\perp)$, where $\Delta p_\perp(t_n) = p_\perp(t_n) - p_\perp(t_{n-1})$, and $t_n - t_{n-1} = 0.17\tau_{ce}$. Mean, standard deviation and skewness are shown from top to bottom. The pdf is generated from 20 macroparticles exhibiting similar trajectories to those shown in Fig. 1. The percentage error on these quantities can be estimated as $\sim 100 \times N^{-1/2} \sim 25\%$.

reflects the fact that the pdf of $\Delta p_\perp$, $g(\Delta p_\perp)$, slowly becomes positively skewed with net positive mean under the effect of the ADI, while also becoming more spread out. This corresponds to the linear phase of the ADI, during which the electrons mostly follow the resonance contour as shown in Fig. 1. The ADI then enters the saturation phase at around $750\tau_{ce}$, after which the mean and skewness decline.

We now turn to the electron mirroring during the saturation phase of the ADI, which is observed in three of the four electron trajectories in Fig. 1. It is helpful to plot the trajectory of a single electron (computationally a macroparticle) overlaid on the electron distribution function in $(v_{||}, x)$ phase space, as shown in Fig. 4. The velocity of electrons under the influence of each Fourier component of an oscillating electric field varies as $\exp i[kx - \omega_k t]$, since waves with a broad

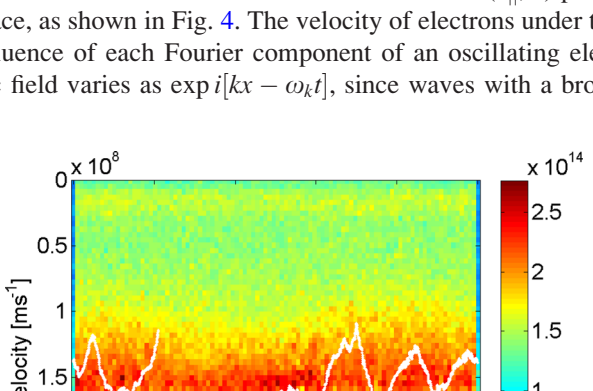

FIG. 4. Trapping and bouncing of an electron with mean pitch angle of 0.9 during the saturation phase of the ADI. The background of this figure is the tail electron distribution in $(v_{||}, x)$ space, where x is the position of the electrons, and the white trace represents the position of a test electron. The colour of the background represents the concentration of electrons in $(v_{||}, x)$ space; red and blue correspond to high and low density respectively. This test electron corresponds to the particle in the top-right panel of Fig. 1. The background is captured at $830\tau_{ce}$ and the trajectory of the electron is plotted from $t = 660 - 1000\tau_{ce}$.

band of wavenumbers k are excited during the ADI. It follows that there is a concentration of particles in $(v_{||}, x)$ space, such that the quasilinear approximation is no longer valid. The electron trajectories become stochastic and can "jump" between resonances in the velocity space. The background of Fig. 4 is a snapshot of the tail electron distribution at $830\tau_{ce}$ and the white trace is the trajectory of the electron in $(v_{||}, x)$ space during the time interval from $660\tau_{ce}$ to $1000\tau_{ce}$. Figure 4 suggests that we should expect an electron to exhibit this kind of mirroring behaviour if it enters into the high concentration band, with $v_{||} \simeq (1.3\text{–}1.7) \times 10^8\,\mathrm{ms}^{-1} \simeq (7.5\text{–}10)v_B$, where v_B is the thermal velocity of the bulk electron population. This would also explain why no such behaviour is observed in the bottom-left panel in Fig. 1, for which the velocity of the electron remains outside the high concentration band throughout the simulation. Physically, the distribution of suprathermal electrons in $(v_{||}, x)$ phase space, in this nonlinear phase of the ADI, must correlate with the parallel phase velocity and spatial location of the excited fields which are supported by these electrons. Trapping and mirroring require approximate resonance between $v_{||}$ and phase velocity, together with significant field amplitudes. The correlation seen in Fig. 4, between the mirroring electron trajectory and the band of high concentration of tail electrons, is thus physically consistent.

B. Quasilinear diffusion

We have seen in the previous subsection A that electron trajectories in $(v_\perp, v_{||})$ space roughly follow the resonance contours defined by Eq. (15), at least until trapping occurs.

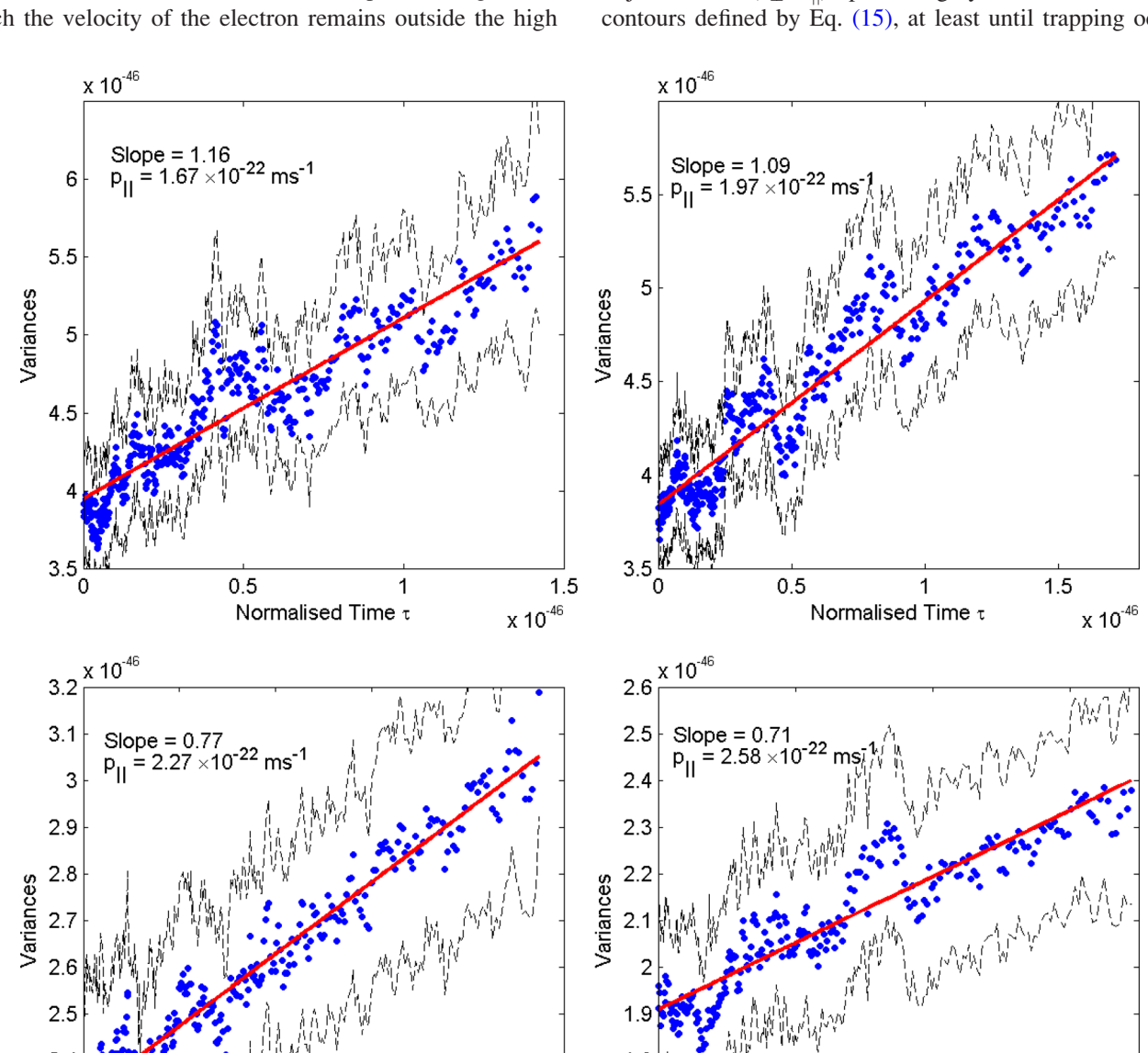

FIG. 5. Variance of the perpendicular momentum distribution plotted against normalised time τ, defined by Eq. (13), for four different parallel momenta in the electron tail, showing approximately quasilinear spreading. Blue dots are the estimated variances at different $p_{||}$, black dashed lines represent the error bands, and red lines show the least squared linear fit.

In this section, we focus on the macroscopic behaviour of the perpendicular momentum distribution of tail electrons at a specific parallel momentum p_s, which can be expressed as

$$\tilde{f}(p_\perp, p_s) = \lim_{\Delta p \to 0} \int_{p_\parallel = p_s - \Delta p}^{p_\parallel = p_s + \Delta p} f(p_\perp, p_\parallel) dp_\parallel. \quad (16)$$

From Eq. (12), we would expect the second order moments, $\sigma^2(p_s) = \int dp_\perp (p_\perp - \bar{p}_\perp)^2 \tilde{f}(p_\perp, p_s)$ to increase linearly with the normalised time τ. Figure 5 shows the second order moments of the perpendicular distribution function, $\tilde{f}$, plotted against normalised time τ for four different parallel momenta p_s. The black dashed line represents the error bounds of the variances and the red lines are the least squared linear fits to the variances. The second order moments of $\tilde{f}$ are calculated from the variances of test particles and the error bars are estimated through bootstrapping, these test particles are samples of the electron distribution f in momentum space. The normalised time in Eq. (13) is calculated using the analytical growth rates γ_k as defined in Ref. 8. These are inserted in the exponential formula for electric field growth at early times, $|E_{k_\parallel}|^2 = |E_0|^2 e^{2\gamma_k t}$, where the initial electrostatic field energy $W_0 = \frac{1}{2}\epsilon_0 |E_0|^2$ where k_B is the Boltzmann constant and T is the bulk electron temperature.

The linear fits in Fig. 5 confirm the linear relationship between the second order moments and the normalised time τ. This is an indication that the simulation results are in good agreement with the quasilinear equation Eq. (12) for the time period shown in Fig. 5, which corresponds to 40–70τ_{ce} in real time and is equivalent to 1.5–3 e-folding times for the fastest growing mode. It is also observed that for higher momentum values, the duration of linear correlation between variances and normalised time is shorter.

Figure 6 shows the vector field $\mathbf{P}(p_{||}, p_\perp, t)$ at $t = 500\tau_{ce}$, which is locally defined as the momentum increment $\mathbf{p}(t_{n+1}) - \mathbf{p}(t_n)$ for $t_{n+1} - t_n = 30\tau_{ce}$, in $(p_{||}, p_\perp)$ space. This vector field governs how $\delta f(p_{||}, p_\perp)$ evolves locally with time in momentum space. It can be observed from the vector field $\mathbf{P}$ that $\mathbf{P} \sim |\mathbf{P}|\hat{e}_\perp$ in the electron tail, where $\hat{\mathbf{e}}_\perp$ is the unit vector along the $p_\perp$ direction. This supports the earlier assumption of the simplified quasi-linear equation, Eq. (12), that the perpendicular evolution of the distribution function is dominant in the quasilinear phase.

IV. CONCLUSIONS

We have analysed the evolution of a minority energetic electron population in phase space under the selfconsistent action of the ADI. Electron trajectories during different stages of the ADI are captured and, in the linear stage, these largely follow the resonance contour. Towards the saturation phase, stochastic electron motion in momentum space is observed. This can be explained by the observed excitation of waves with a broad band of wavenumber k. The relationship between the second order moments of the perpendicular electron distribution function and time is established. During the linear phase of the ADI, these are in good agreement with the quasilinear theory but thereafter, trapping and mirroring dynamics come into play.

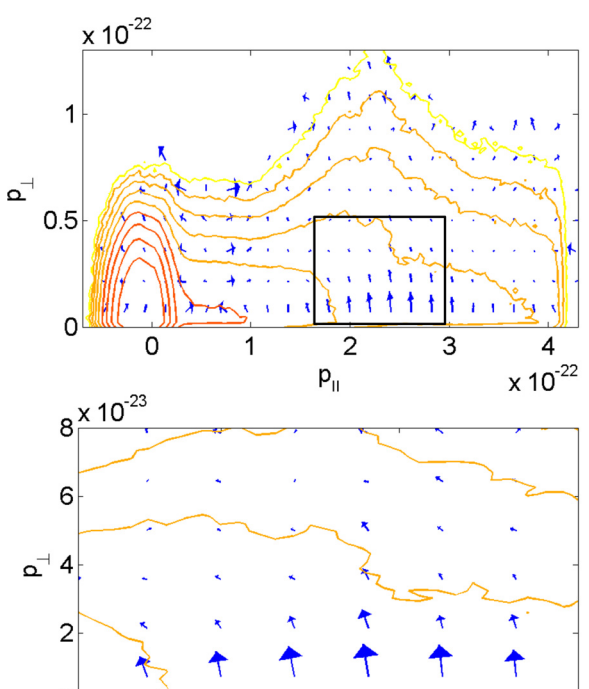

FIG. 6. Top panel shows the vector field $\mathbf{P}$ of increments in $(p_{||}, p_\perp)$ momentum space, overlaid on logarithmic constant-f contour plots of the electron distribution at $500\tau_{ce}$. Bottom panel focuses on the tail population in the top panel, corresponding to the region marked there by a rectangle. The length of the arrows is scaled for clearer representation.

ACKNOWLEDGMENTS

This work has received funding from the European Union's Horizon 2020 research and innovation programme under Grant agreement number 633053 and was part-funded by the RCUK Energy Programme under Grant EP/I501045. The views and opinions expressed herein do not necessarily reflect those of the European Commission. The EPOCH code used in this work was developed as part of an EPSRC funded Project, Grant number EP/G054950/1.

[1]B. B. Kadomtsev and O. P. Pogutse, Sov. Phys. JETP **26**, 1146 (1968).
[2]V. D. Shapiro and V. I. Shevchenko, Sov. Phys. JETP **27**, 635 (1968).
[3]R. O. Dendy and C. N. Lashmore-Davies, Plasma Phys. **26**, 1347 (1984), available at http://iopscience.iop.org/article/10.1088/0741-3335/26/11/009.
[4]R. O. Dendy, Phys. Fluids **30**, 2438 (1987).
[5]R. O. Dendy, C. N. Lashmore-Davies, and M. M. Shoucri, Nucl. Fusion **25**, 721 (1985).
[6]L. Muschietti, K. Appert, and J. Vaclavik, Phys. Fluids **24**, 151 (1981).
[7]L. Muschietti, K. Appert, and J. Vaclavik, Plasma Phys. **24**, 987 (1982).
[8]R. O. Dendy, C. N. Lashmore-Davies, and A. Montes, Phys. Fluids **29**, 4040 (1986).
[9]W. N. Lai, S. C. Chapman, and R. O. Dendy, Phys. Plasmas **20**, 102122 (2013).
[10]K. Molvig, M. S. Tekula, and A. Bers, Phys. Rev. Lett. **38**, 1404 (1977).
[11]S. C. Liu, V. S. Chan, D. K. Bhadra, and R. W. Harvey, Phys. Rev. Lett. **48**, 1479 (1982).
[12]S. C. Luckhardt, K.-I. Chen, M. J. Mayberry, M. Porkolab, Y. Terumichi, G. Bekefi, F. S. McDermott, and R. Rohatgi, Phys. Fluids **29**, 1985 (1986).

[13]K. Ronald, S. L. McConville, D. C. Speirs, A. D. R. Phelps, C. W. Robertson, C. G. Whyte, W. He, K. M. Gillespie, A. W. Cross, and R. Bingham, Phys. Plasmas **15**, 056503 (2008).
[14]K. Ronald, S. L. McConville, D. C. Speirs, A. D. R. Phelps, C. W. Robertson, C. G. Whyte, W. He, K. M. Gillespie, A. W. Cross, and R. Bingham, Plasma Sources Sci. Technol. **17**, 035011 (2008).
[15]R. Bingham, R. A. Cairns, I. Vorgul, and V. D. Shapiro, J. Plasma Phys. **76**, 539 (2010).
[16]G. O. Pokol, A. Kómár, A. Stahl, and T. Fülöp, Phys. Plasmas **21**, 102503 (2014).
[17]S. Sajjad, X. Gao, B. Ling, S. H. Bhatti, and T. Ang, Phys. Plasmas **17**, 042504 (2010).
[18]Y. M. Wang, X. Gao, L. Ling, Y. Liu, S. B. Zhang, X. Han, A. Ti, E. Z. Li, and HT-7 Team, Phys. Plasmas **19**, 032509 (2012).
[19]S. J. Freethy, K. G. McClements, S. C. Chapman, R. O. Dendy, W. N. Lai, S. J. P. Pamela, V. F. Shevchenko, and R. G. L. Vann, Phys. Rev. Lett. **114**, 125004 (2015).
[20]H. A. S. Reid, Res. Astron. Astrophys. **14**, 773 (2014).
[21]R. O. Dendy, Plasma Phys. Controlled Fusion **33**, 1069 (1991).
[22]V. V. Parail and O. P. Pogutse, Sov. J. Plasma Phys. **2**, 126 (1976).
[23]J. W. S. Cook, S. C. Chapman, and R. O. Dendy, Phys. Rev. Lett. **105**, 255003 (2010).
[24]For a fully documented version of this code, see https://ccpforge.cse.rl.ac.uk/gf/project/epoch.
[25]P. Aleynikov and B. N. Breizman, Nucl. Fusion **55**, 043014 (2015).
[26]W. Horton, P. Zhu, G. T. Hoang, T. Aniel, M. Ottaviani, and X. Garbet, Phys. Plasmas **7**, 1494 (2000).
[27]C. F. Kennel and F. Engelmann, Phys. Fluids **9**, 2377 (1966).
[28]R. M. Kulsrud and A. Ferrari, Astrophys. Space Sci. **12**, 302–318 (1971).
[29]T. H. Stix, *Waves in Plasmas* (AIP Publishing, New York, 1992).
[30]A. B. Mikhailovskii, *Theory of Plasma Instabilities, Vol 1: Instabilities of a Homogeneous Plasma* (Springer, 1974).
[31]R. Koch, Plasma Phys. Controlled Fusion **48**, B329 (2006).
[32]C. F. F. Karney, Comput. Phys. Rep. **4**, 183 (1986).
[33]C. S. Liu and Y. Mok, Phys. Rev. Lett. **38**, 162 (1977).
[34]T. Fülöp, G. Pokol, P. Helander, and M. Lisak, Phys. Plasmas **13**, 062506 (2006).
[35]G. Pokol, T. Fülöp, and M. Lisak, Plasma Phys. Controlled Fusion **50**, 045003 (2008).
[36]E. Marsch and C. Y. Tu, J. Geophys. Res. **106**, 227, doi:10.1029/2000JA000042 (2001).
[37]D. B. Melrose, *Instabilities in Space and Laboratory Plasmas* (Cambridge University Press, 1986).
[38]F. Castejon and S. Eguilior, Technical Report, CIEMAT-1015, 2003.